AD-A181 217 JOURNAL OF CHINA UNIVERSITY OF SCIENCE AND TECHNOLOGY 1/1
(SELECTED ARTICLES)(U) FOREIGN TECHNOLOGY DIV
WRIGHT-PATTERSON AFB OH 18 MAY 87 FTD-ID(RS)T-0208-87

UNCLASSIFIED F/G 20/4 NL

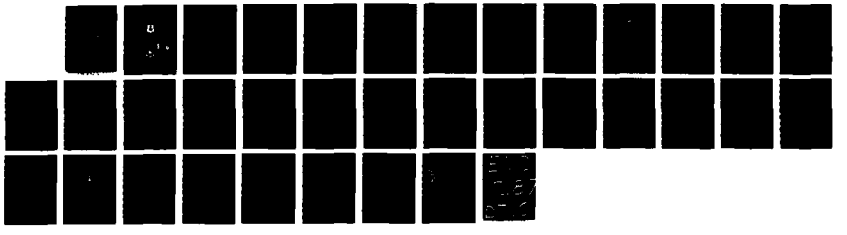

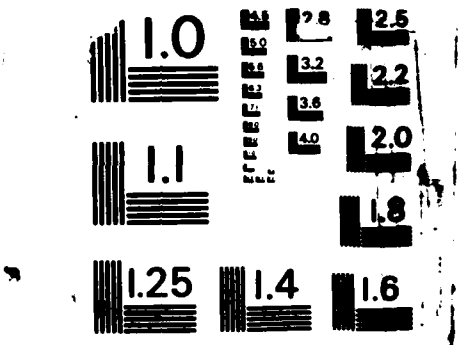

FTD-ID(RS)T-0208-87

FOREIGN TECHNOLOGY DIVISION

JOURNAL OF CHINA UNIVERSITY OF SCIENCE AND TECHNOLOGY

(Selected Articles)

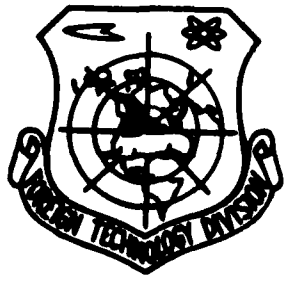

HUMAN TRANSLATION

FTD-ID(RS)T-0208-87 18 May 1987

MICROFICHE NR: FTD-87-C-000358

JOURNAL OF CHINA UNIVERSITY OF SCIENCE AND TECHNOLOGY
(Selected Articles)

English pages: 29

Source: Ke Daxue Xuebao, Vol. 16, Nr. 1, March 1986, pp. 66-77

Country of origin: China
Translated by: SCITRAN
F33657-84-D-0165
Requester: FTD/TQTA

PREPARED BY:

TRANSLATION DIVISION
FOREIGN TECHNOLOGY DIVISION
WPAFB, OHIO.

TABLE OF CONTENTS

GRAPHICS DISCLAIMER

All figures, graphics, tables, equations, etc. merged into this translation were extracted from the best quality copy available.

Effect of Nose Bluntness on Twin Wave Interference /66

Xia Nan and Chen Qiang

(Department of Modern Mechanics)

Abstract

This paper discusses the mutual interaction between an oblique blast wave and the shock wave layer on a supersonic blunt cone. A flow field superposition technique is used to calculate the shape of the transmitted blast wave and peak pressure produced as it is reflected on the cone. A detailed analysis shows that due to the complexity of the blunt cone flow field, especially the effect of the high entropy layer, the shapes of the transmitted blast wave and the peak pressure are quite different from those obtained with a slender one.

When a supersonic blunt cone encounters a planar blast wave, the planar blast wave meets the bow-shaped separated shock wave of the blunt cone. A transmitted blast wave is propagating in the shock wave layer of the blunt cone. The transmitted blast wave is reflected from the surface of the blunt cone. This is the so-called "twin wave interference".

The "twin wave interference" problem has an important practical significance in the aerodynamic design of a high speed

---

Manuscript received on May 25, 1985

vehicle. Since the 1960's a lot of work has been done in theoretical analysis and experimental research. References [1] and [2] give a good overall summary. As for the twin wave interference involving a sharp cone, because the interference flow field is similar, the problem is greatly simplified. Good results have been obtained in engineering as well as in numerical computation. In the twin wave interference problem with a supersonic blunt object, however, because the flow field of a slender blunt cone is far more complex than that of a sharp cone, all engineering computation techniques are limited to the stationary point region. Numerical calculation[3] is also limited to the blunt tip region[4,5]. Moreover, it consumes quite a bit of computer time.

The purpose of this paper is to expand the flow field superposition technique reported in the references [2,6] to the interaction between an oblique blast wave and the shock wave layer of a blunt cone. The paper discusses the peak pressure variation on the cone as affected by the small blunt head. It is also compared to the situation of a sharp cone.

In order to simplify the study, we only considered a zero attack angle blunt cone. We also limited ourselves to the flow within the meridian plane. It is assumed that the gas is an ideal gas with a constant specific heat, r=1.4. All parameters in the paper are dimensionless. The velocity, pressure and density are relative to incoming flow velocity a_x, pressure P_∞ and density p_∞, respectively. The length is relative to the

radius of the spherical head r_b. The entropy is relative to the gas constant R.

I. Calculation of High Speed Blunt Cone Flow Field Parameter Before Interference

Numerical solution is used to represent the initial flow field of the blunt cone before interference. In the hybrid flow region in the head area, a linear method was used[7]. In the rear supersonic region, an eigenline method was used[8]. If x is axial distance from the body axis from the center of the spherical head and r is the distance from a point in the flow field to the body axis, let us define the coordinate ξ,

/67

$$\xi = \frac{r - r_w(x)}{r_s(x) - r_w(x)}, \qquad (1)$$

where $0 \leq \xi \leq 1$. The subscript s represents a shock wave value and w represents a surface value. Let us transform the r, x coordinate to ξ, x, and divide the shock wave layer into N layers along the r-direction and express them as ξ_i where $1 = \xi_S = \xi_1 > \xi_2 \ldots > \xi_{N+1} = \xi_w = 0$. In the x-direction, let us choose K straight lines where x are constants $x_1 < x_2 < \ldots x_k$. Then, let us divide the entire shock wave layer into meshes as shown in Figure 1. We used an intrapolation technique to determine the parameters at the nodal points (ξ_i, x_j) of the network. In calculating the supersonic flow field in the rear of the object, we only went as far as x=15. Within the

range of parameters calculated, the results agreed quite well with other people's values[9]. Figure 2 shows the surface pressure and Mach number distribution along the x-direction when M_∞=4 and the semi-cone angle δ=10°. From the figure we can see that the sharp cone has a constant surface pressure, while a blunt cone has an over exposure characteristic. The lowest pressure is smaller than the pressure on a sharp cone. Then, it gradually rises back to the sharp cone value. Because of the high temperature in the high entropy layer, the speed of sound on the surface of a blunt cone is much larger than that on a sharp cone. Hence, the Mach number of the flow is much less than the sharp cone case. Figure 3 shows how the flow parameters vary along the ξ direction when x=5. The figure also indicates that in the case of a sharp cone, it is a isoentropic compression process from the shock wave to the surface of the object. Therefore, both density and pressure are increased. As for a blunt cone, because of the high entropy layer on the surface, the density at the surface is much lower than that behind the shock wave.

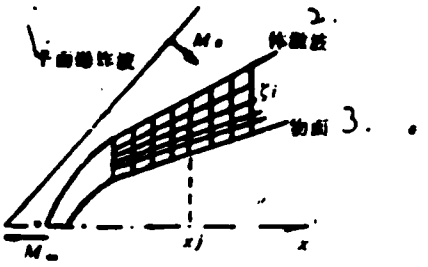

Figure 1 Division of the Flow Field Meshes

1. planar blast wave
2. body shock wave
3. surface

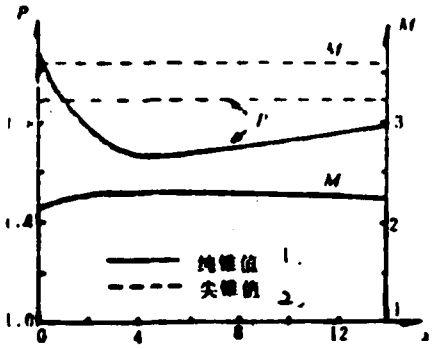

Figure 2 Pressure Distribution on the Surface of a Blunt Cone $M_\infty=4\ \delta=10^o$

1. sharp cone
2. blunt cone

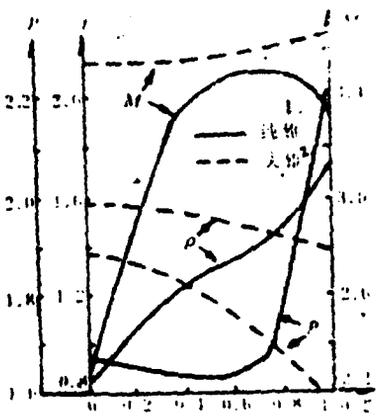

Figure 3 Variation of Blunt Cone Shock Wave Layer Parameters in Three Directions, $M_\infty=4$, $\delta=10^O$, $x=5$

1. blunt cone
2. sharp cone

II. Interference Between Planar Blast Wave and Blunt Cone Shock Wave Layer

When a planar blast wave traveling at a Mach number M_B encounters a supersonic blunt cone at an encounter angle θ_B (which is defined as the angle between the blast wave and a line perpendicular to the body axis on the meridian plant where $\Phi=0$), it is certain that the blast wave collides with the body shock wave first. It creates two new shock waves which are called transmitted blast wave and transmitted body shock wave, respectively. There is a contact surface between them. Then, the transmitted blast wave is reflected by the surface of the dull cone through the entire shock wave layer. Here, we will primarily discuss the formation of this twin wave interference : the supersonic region of the cone, as shown in Figure 4.

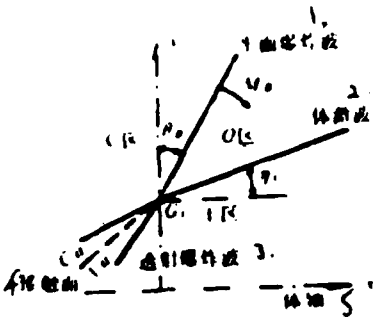

Figure 4 Encounter Between Planar Blast Wave and Blunt Cone Shock Wave

1. planar blast wave
2. body shock wave
3. transmitted blast wave
4. contact surface
5. transmitted body shock wave

At a certain instance, the planar blast wave meets the curved body shock wave at point G_1. In the body axis coordinate system the velocity of G_1 moving in the tangential direction of the body shock wave can be expressed as

$$V_{G_1} = \frac{M_2 + M_\infty \cos\theta_2}{\cos(\theta_2 + \eta_1)}, \tag{2}$$

Its components in the X and Y directions, respectively, are

$$V_{G_1 x} = V_{G_1} \cos\eta_1, \tag{3}$$

$$V_{G_1 y} = V_{G_1} \sin\eta_1, \tag{4}$$

where η_1 is the angle of inclination of the body shock wave at G_1, i.e. β. In the body coordinate system, the parameters in region C following the planar blast wave can be expressed as

$$u_{c,s} = M_\infty + \left(1 - \frac{1}{\rho_c}\right) M_s \cos\theta_s, \tag{5}$$

$$u_{c,n} = -\left(1 - \frac{1}{\rho_c}\right) M_s \sin\theta_s, \tag{6}$$

$$\frac{1}{\rho_c} = \frac{2}{\gamma+1}\left(\frac{1}{M_s^2} + \frac{\gamma-1}{2}\right), \tag{7}$$

$$P_c = \frac{2\gamma}{\gamma+1} M_s^2 - \frac{\gamma-1}{\gamma+1}, \tag{8}$$

The flow field parameters in region 1 immediately after point G_1 have been obtained from the numerical solution. If the coordinate system is fixed on point G_1, based on the relation that the pressure is equal on either side of the contact surface and the flow direction is consistent, we get

$$\frac{\frac{2\gamma}{\gamma+1}(M_1 \sin\varphi_1)^2 - \frac{\gamma-1}{\gamma+1}}{\frac{2\gamma}{\gamma+1}(M_c \sin\varphi_c)^2 - \frac{\gamma-1}{\gamma+1}} = \frac{P_c}{P_1}, \tag{9}$$

$$tg^{-1}\left[\frac{M_1'^2\sin\varphi_1\cos\varphi_1-ctg\varphi_1}{1+M_1'^2\left(\frac{\gamma+1}{2}-\sin^2\varphi_1\right)}\right]+tg^{-1}\left[\frac{M_c'^2\sin\varphi_c\cos\varphi_c-ctg\varphi_c}{1+M_c'^2\left(\frac{\gamma+1}{2}-\sin^2\varphi_c\right)}\right]$$

$$=\lambda_C'-\lambda_1' \qquad (10)$$

where M_1', λ_1' and M_C', λ_C' are the Mach number and deflection angle relative to a coordinate system fixed at G_1 for Region 1 and Region C, respectively.

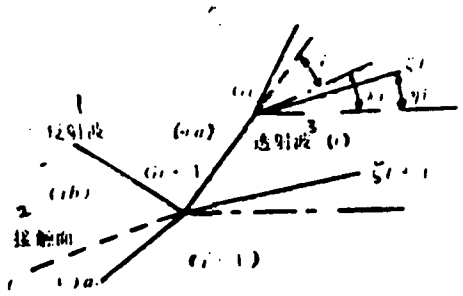

Figure 5 Refraction and Reflection of Blast Wave on Various Interfaces

1. blast wave
2. contact surface
3. transmitted wave

φ_1 and φ_C are the angles of inclination of the flow in region 1 with respect to the transmitted blast wave transmitted body shock wave, respectively. Based on these two equations, φ_1 and φ_C can be determined. /69

With a sharp cone, the twin wave interference flow field is similar to the flow field itself. The transmitted blast wave moves at a constant speed along a line coming out of the apex. The shape of the transmitted wave is similar at different x positions. In the case of a blunt cone, the similarity does not exist. At different x positions, the shape of the transmitted blast wave is different. We divided the entire shock wave layer into N thin layers based on the coordinate ξ. In a small region within ξ_i to ξ_{i+1} and X_j to X_{j+1}, the transmitted blast wave is approximated as a straight line. The wavefront parameters are obtained based on the local numerical solution. It moves in parallell at a speed V_{Gi} (see Figure 5). If a physical quantity on the i^{th} layer is known, then it is possible to calculate it in the $i+1^{th}$ layer. If φ_i is known, the angle between the transmitted wave from the i^{th} layer and the x-axis, φ_{ix}, is

$$\varphi_{i,x} = \varphi_i + \lambda_i \qquad (11)$$

Based on this equation, it is possible to obtain the intersect between the transmitted blast wave and ξ_{i+1}, G_{i+1} and the coordinates of this point (ξ_{i+1}, X_{i+1}). Let η_i be the angle between the tangent of ξ_i and the x-axis. Then, the velocity of G_{i+1} moving along the tangent of ξ_{i+1}, V_{Gi+1}, can be written as

$$V_{G,i+1} = V_{G,i} \frac{\sin(\varphi_{i,x} - \eta_i)}{\sin(\varphi_{i,x} - \eta_{i+1})}, \qquad (12)$$

$$\eta_{i+1} = \operatorname{tg}^{-1} \frac{y_{i+1,j+1} - y_{i+1,j}}{X_{i+1} - X_i}, \qquad (13)$$

where

$$X_j \leq X_{(i+1)} < X_{j+1}$$

The transmitted blast wave is refracted after meeting the interface ξ_{i+1} at G_{i+1}. In addition, an isoentropic wave is reflected. There is a contact surface between the isoentropic wave the transmitted wave layer in the $i+1^{th}$ layer. The shape of wave and the transmitted in the $i+1^{th}$ layer should meet the condition that the pressure on either side of the contact surface is equal and the direction of velocity is consistent. The wave front parameters in the i^{th} and $i+1^{th}$ regions are known. The shock wave shape in the i^{th} layer is already known. The parameters behind the wave in region ia can be determined. The shape of the reflected wave and the shape of the transmitted wave in the $i+1^{th}$ layer can be found based on two compatible conditions; i.e. it is possible to obtain φ_{i+1}. To simplify the computation, a small parameter expansion formula may be used to derive an iterative formula. The transmitted waves of the i^{th} and $i+1^{th}$ layer can be obtained based on the oblique shock wave relation. The isoentropic wave employs a simple wave relationship. The following functions are defined by us

$$\frac{P_a}{P} = F_1(M,\gamma,\varphi), \tag{14}$$

$$\lambda_a - \lambda = F_2(M,\gamma,\varphi), \tag{15}$$

$$\frac{\gamma M_a^2}{\sqrt{M_a^2-1}} = F_3(M,\gamma,\varphi), \tag{16}$$

The subscript a indicates parameters behind the wave.

If the coordinate system is fixed at the intersect G_{i+1}, the following equation can be derived based on the compatibility relation of the contact surface.

$$F_1(M'_{i+1},\gamma,\varphi_{i+1}) = \{1-F_2(M'_i,\gamma,\varphi_i)[\lambda'_{i+1}-\lambda'_i+F_2(M'_{i+1},\gamma,\varphi_{i+1}) - F_2(M'_i,\gamma,\varphi_i)]\}F_1(M'_i,\gamma,\varphi_i)\frac{P_i}{P_{i+1}}, \tag{17}$$

The parameters of two neighboring layers differ insignificantly. Let

$$P_{i+1} = P_i + dP, \tag{18}$$

$$\lambda'_{i+1} = \lambda'_i + d\lambda', \tag{19}$$

$$F_n(M'_{i+1},\gamma,\varphi_{i+1}) = F_n(M'_i,\gamma,\varphi_i) + dF_n, \quad (n=1,2,3), \tag{20}$$

By substituting these equations into equation (17), we get

/70

$$\frac{dF_1}{F_1} = -F_2(d\lambda' + dF_2) - \frac{dP}{P}, \tag{21}$$

where

$$dF_1 = \frac{\partial F_1}{\partial \varphi}d\varphi + \frac{\partial F_1}{\partial M'}dM',$$

$$dF_2 = \frac{\partial F_2}{\partial \varphi}d\varphi + \frac{\partial F_2}{\partial M'}dM',$$

By substituting these equations into equation (21) and changing it from a differential to a difference equation, we finally get

$$\varphi_{i+1} - \varphi_i = -\frac{\left(\frac{1}{F_1}\frac{\partial F_1}{\partial M_i'} + F_s\frac{\partial F_s}{\partial M_i'}\right)(M_{i+1}' - M_i') + F_s(\lambda_{i+1}' - \lambda_i') + \left(\frac{P_{i+1}}{P_i} - 1\right)}{\frac{1}{F_1}\frac{\partial F_1}{\partial \varphi_i} + F_s\frac{\partial F_s}{\partial \varphi_i}}, \qquad (22)$$

where M_i', λ_2' and $1/F_1\ \partial F_1/\partial M_i'$, $\partial F_2/\partial M_i'$, $\partial F_2/\partial \varphi_i$, $1/F_1\ \partial F_1/\partial \varphi_i$, F_s are shown in equation (3-12) in reference [2]. The relative Mach number and inclination angle of the flow behind the transmitted blast wave are:

$$M_{i+1}'^2 = \frac{(\gamma-1)M_i'^2+2}{2\gamma M_i'^2\sin^2\varphi_i - (\gamma-1)} + \frac{2M_i'^2\cos^2\varphi_i}{(\gamma-1)M_i'^2\sin^2\varphi_i + 2}, \qquad (23)$$

$$\lambda_{i+1}' = \lambda_i' + \operatorname{tg}^{-1}\left[\frac{M_i'^2\sin\varphi_i\cos\varphi_i - c\operatorname{tg}\varphi_i}{1+M_i'^2\left(\frac{\gamma+1}{2} - \sin^2\varphi_i\right)}\right], \qquad (24)$$

The angle between the transmitted blast wave and the x-axis is expressed in equation (11).

As we proceed making the calculation layer by layer, when we reach the layer closest to the cone surface which is the N^{th} layer (see Figure 6), the angle between the transmitted blast

wave and the cone surface θ_a (which is the incident angle) is approximately equal to φ_N. If θ is the angle of deflection of the flow passing through the transmitted wave, it should also be the deflection angle of the flow passing through the reflected wave.

$$\theta = \lambda_{Na} - \delta \tag{25}$$

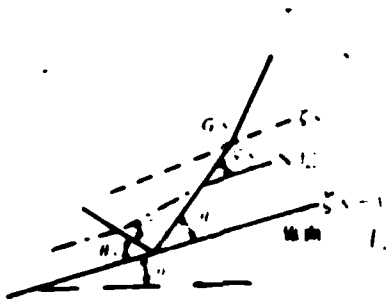

Figure 6 Reflection of Transmitted Blast Wave on the Surface

1. cone surface

The maximum deflection angle of the flow after passing through the reflected shock wave is

$$\theta_{max} = \operatorname{tg}^{-1}\left[\operatorname{ctg}(\varphi_1)_* \frac{M_{N2}'^2 \sin^2(\varphi_1)_* - 1}{1 + M_{N2}'^2\left(\frac{\gamma+1}{2} - \sin(\varphi_1)_*\right)}\right], \tag{26}$$

where $(\varphi_1)_*$ is the maximum deflection angle of the flow. The angle of inclination of the corresponding maximum reflected

shock wave is determined by the following equation:

$$\sin^2(\varphi_1)_{\max} = \frac{1}{\gamma M_{N1}^2}\left[\frac{\gamma-1}{4}M_{N1}^2 - 1 + \sqrt{(\gamma+1)\left(1+\frac{\gamma-1}{2}M_{N1}^2+\frac{\gamma+1}{16}M_{N1}^4\right)}\right], \quad (27)$$

If $\theta_{max} > \theta$, then it is a routine reflection. The following /71
equation must be first used to determine the angle of inclination φ_1 of the reflected shock wave.

$$\operatorname{tg}\theta = \operatorname{ctg}\varphi_1 \frac{M_{N1}^2\sin^2\varphi_1 - 1}{1+M_{N1}^2\left(\frac{\gamma+1}{2}-\sin^2\varphi_1\right)}, \quad (28)$$

The pressure behind the reflected shock wave is

$$\frac{P_N}{P_{N1}} = \frac{2\gamma}{\gamma+1}M_{N1}^2\sin^2\varphi_1 - \frac{\gamma-1}{\gamma+1}, \quad (29)$$

The angle between the reflected shock wave and the cone surface (angle of reflection)

$$\theta_1 = \varphi_1 - \theta \quad (30)$$

If $\theta_{max} < \theta$, it must be a Mach type of reflection. The pressure behind the wave is calculated by the following equation:

$$\frac{P_{2N}}{P_N} = \frac{2\gamma}{\gamma+1}M_N^2 - \frac{\gamma-1}{\gamma+1}, \quad (31)$$

There is another case (Figure 5). When the computation proceeds

to point G_{i+1}, if the Mach number is in zone ia behind the wave $M'_{ia}<1$ relative to the coordinate fixed at G_{i+1}, i.e. the flow is subsonic, it is not possible to produce a reflected wave. In this situation, we can assume that a Mach reflection is produced at point G_i. Make a line perpendicular to the surface at G_i. Its intersection at the surface G_N is used to calculate the surface pressure behind the normal shock wave.

Our calculation showed that there is little difference between the results obtained based on the iterative equation (22) and the results obtained with a rigorous shock wave simple wave relationship by trial iterations.

III. Calculated Results and Discussion

Based on the method discussed in this paper, we performed computations on a Chinese made Model 320 computer in two cases; $M_\infty=4$, $\delta=10^\circ$, $M_B=2$ and $M_\infty=5$, $\delta=11.2^\circ$, $M_B=2$.

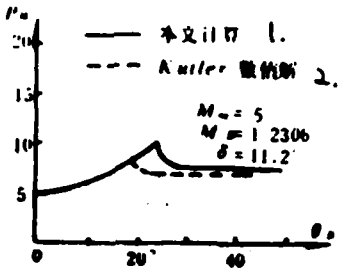

Figure 7 Oblique Interference Pressure on a Sharp Cone with θ_B

1. this work
2. numerical solution done by Kutler

$M_\infty = 5$, $M_2 = 1.2306$, $\delta = 11.2°$

Figure 8 Oblique Interference Pressure on a Blunt Cone with θ_B

1. sharp cone

Due to the complexity of the twin wave interference involving a blunt cone, we have not yet seen any theoretical and experimental results to date for comparison. For this reason, the oblique interference pressure on a sharp cone calculated with this method is shown in Figure 7 together with the numerical solution obtained by Kutler[10,11] for comparison. The agreement appears to be reasonable. Figures 8 and 9 show the calculated peak pressure and geometric shape of the transmitted blast wave from the interaction between an oblique blast wave and a high speed cone, respectively. For comparison, the calculated value of a sharp cone is also plotted. From Figure 8 we can see that the peak pressure on a blunt cone is much lower than that on a sharp cone under similar conditions. This apparently is due to the high entropy layer near the surface. The high speed of sound associated with the high temperature makes the Mach number of the flow near the surface much lower than that of the transmitted blast wave. In the figure, X_s is the coordinate of the intersect between the blast wave and the shock wave G_1. From the Figure we /72
can also see that when the Mach number M_∞ increases, this entropy layer effect becomes more pronounced. The peak pressure of a sharp cone is independent of the axial position. The flow field of a blunt cone varies with the axial position. Thus, the peak pressure also varies. The figure also shows the angle θ_b^*, at which it changes from routine reflection to Mach reflection. In the case of a blunt cone, it is less than that with a sharp cone.

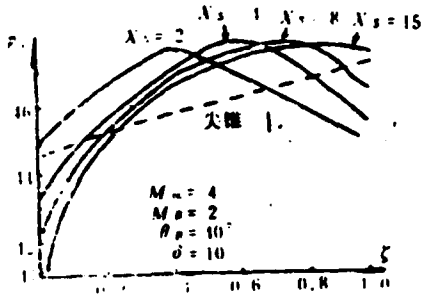

Figure 9 Transmitted Blast Wave With a Blunt Cone in Oblique Interaction vs. Body Axis Angle ξ

1. sharp cone

Figure 9 shows the geometric shape of the transmitted blast wave with a blunt cone during oblique interference. The figure shows that the slope of the transmitted blunt wave in the shock wave layer of a sharp cone is decreasing uniformly. In the case of a blunt cone, the shape of the transmitted blast wave also varies quite a bit. This is particularly true as the point X_s gets closer to the shoulder of the blunt cone. As X_s increases, ϕ_x gradually decreases monotonically. However, because the entropy layer gradient is larger near the surface, ϕ_x decreases faster.

When using this method to calculate the twin wave interference on a blunt cone, it takes approximately 30 minutes to compute the steady flow field. It only takes 1-2 minutes to calculate a set of θ_B values (24 values) with a set of given X_x and M_B. With respect to a given set of M_∞ and δ, the steady flow field calculated does not have to be repeated for varying X_s, M_B and θ_B in calculating the interference flow field.

IV. Conclusions

The flow field superposition technique introduced in reference [2] was used to solve the mutual interference between an oblique blast wave and a high speed blunt cone shock wave layer to determine the geometric shape of the transmitted blast wave and the peak pressure on the surface. The results indicate that because of the high entropy layer formed at the high speed blunt head, the entropy gradient at the surface is very high, the gas temperature and speed of sound are also high. The Mach number of the flow is low, which makes the peak pressure much lower as compared to that with a sharp cone. In addition, due to the inhomogeneity of the flow field, the shape of the transmitted blast wave is also quite different from that associated with a sharp cone.

References

[1] Chen Qiang and Xia Nan, On Computation Methods for the "Twin Wave Interference" Problem, Non-linear Wave Discussion Meeting, Chinese Society of Mechanics, (1981).

[2] Chen Qiang and Xia Nan, Mutual Interaction Between Oblique Blast Wave and Supersonic Spherical Cone, Journal of China University of Science and Technology, 12 (1982), No. 1.

[3] Taylor, T.D., Hudgins, H.E., J. AIAA, 6 (1968), No. 2, 198.

[4] McNamara, W., J. Spacecraft and Rockets, 4 (1967), No. 6, 790.

[5] Champney, J.M., Chaussee, D.S., Kutler, P., AIAA Paper, 82-0227, (1982).

[6] Chen Qiang and Xia Nan, A Method to Calculate the Interaction Between Oblique Blast Wave and Supersonic Spherical Cone, Journal of Aerodynamics, 1982, No. 4.

[7] Gilinskiy,S.M.,Telenin,G.F., AN SSSR, Mekhanika i Mash., 1964, No. 5, 148.

[8] Bian Yinqui editor, Ideal Aerodynamics, Lecture Notes of Chinese University of Science and Technology, 1966.

[9] Zhu Youlan et al, Initial Value Difference Method and Circulation, Science Publishing Co., 1980.

[10] Kutler, P., AIAA, 74-524, (1974).

[11] Kutler, P., AIAA, 75-49, (1975).

Application of Finite Element Method to Transonic Airfoils /74
- A Preliminary Steady Subcritical Calculation

Xu Shoudong and An Changfa
(Department of Modern Mechanics)

Abstract

In this paper, the finite element method developed by Galerkin is used to calculate the surface pressure distribution on a symmetric double curved airfoil. Numerical results basically are in agreement with experimental data.

Based on the transonic small perturbation equations, the finite element method is used to calculate the transonic flow field of a symmetric double curve airfoil. Referring to reference [1], we employed a rectangular mesh scheme and the Hermite interpolation function. The Galerkin method was used to control the error. However, in the finite element analysis, we did not use the numerical integration in determining the values of elements of the unity matrix. Instead, we found an iterative formula to integrate all the elements in the rigidity matrix. Through the calculation of the subcritical pressure distribution of a 6% symmetric airfoil, it was demonstrated that the method is feasible.

Manuscript received on June 6, 1985

I. Theoretical Analysis

The steady transonic flow around a two-dimensional thin airfoil can be described by the transonic small perturbation equations and the associated boundary conditions.

$$[1-M_\infty^2-M_\infty^2(\gamma+1)\phi_x]\ \phi_{xx}+\phi_{yy}=0 \tag{1}$$

$$\phi_y-(1+\phi_x)g'=0 \text{ (on the wing)} \tag{2}$$

$$\phi=0, \text{ (at infinity)} \tag{3}$$

where g(x) is the dimensionless wing surface equation. When $M_\infty \to 1$, it was proven in reference [2] that $M_\infty\sqrt{1+(\gamma+1)\ \phi_x}=M_1^2$ (local Mach number). Then, equation (1) can be written as

$$\phi_{xx}+\phi_{yy}=f, \quad f=M_1^2\phi_{xx} \tag{4}$$

As a preliminary approximation, boundary condition (3) can be considered valid at a finite distance.

If the airfoil is symmetric and the attack angle of the incoming flow is zero, we only have to consider the upper half. Let us choose a rectangular area which is 5 times the chord length and 2 times the chord length height and divide it into 64 elements with 85 nodes as shown in Figure 1. For a thin airfoil, the elements near the wing surface can also be treated as rectangles. By doing the following transformation $\xi=(x-x_c)/a$, $\eta=(y-y_c)/b$, where a, b, (x_c,y_c) are the half length, half height, and center coordinate of a certain element, respectively, then all elements become identical cubic elements as shown in Figure 2. /75

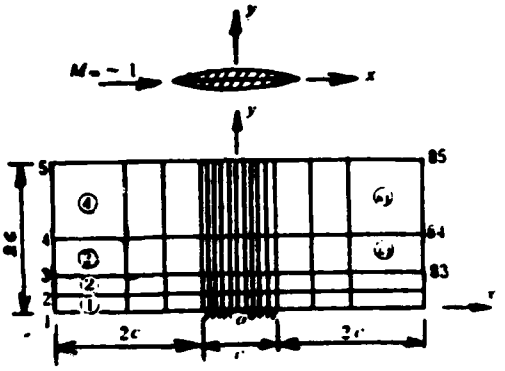

Figure 1

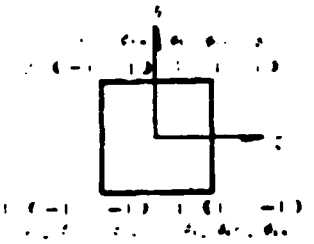

Figure 2

Let's do a Hermite interpolation on the function ϕ in each cubic element

$$\overline{\phi}(\xi,\eta)=\phi_i N_i(\xi,\eta) \qquad (5)$$

where ϕ_i (i=1,2,...,12) represent the functions and derivatives on the nodes: ϕ_1, $\phi_{1\xi}$, $\phi_{1\eta}$, ϕ_2, $\phi_{2\xi}$, $\phi_{2\eta}$, ϕ_3, $\phi_{3\xi}$, $\phi_{3\eta}$, ϕ_4, $\phi_{4\xi}$, $\phi_{4\eta}$. $N_i(\xi,\eta)$ (i=1, 2,...,12) are the shape functions. Their specific expressions can be found in Conner's book[3]. For example:

$$\begin{cases} N_1 = \frac{1}{8}(\eta-1)(\xi-1)\left[\frac{1}{2}(\eta-1)(\xi-1)-\frac{1}{2}(\eta+1)(\xi+1)\right. \\ \qquad \left.-(\eta-1)(\eta+1)-(\xi-1)(\xi+1)\right], \\ \qquad \cdots\cdots\cdots \\ N_3 = -\frac{1}{8}(\eta-1)^2(\eta+1)(\xi-1), \\ \qquad \cdots\cdots\cdots \\ N_4 = -\frac{1}{8}(\eta-1)(\eta+1)^2(\xi-1), \\ \qquad \cdots\cdots\cdots \end{cases} \tag{6}$$

Based on the Galerkin method, we have the following relation in element E and wing surface W:

$$\iint_E (\bar{\Phi}_{xx}+\bar{\Phi}_{yy}-\bar{f})N_i\,dxdy+\int_w[\bar{\Phi}_y-(1+\bar{\Phi}_x)]g'N_i\,dl=0 \tag{7}$$

According to Green theorem, we get

$$\begin{aligned} \iint_E(\bar{\Phi}_x N_{ix}+\bar{\Phi}_y N_{iy})dxdy &= \oint_{ss}\bar{\Phi}_x N_i\,dl-\iint_E M_i^j\bar{\Phi}_{xx}N_i\,dxdy \\ &+\int_w[\bar{\Phi}_y-(1+\bar{\Phi}_x)]g'N_i\,dl=0 \end{aligned} \tag{8}$$

where $\bar{\Phi}_n$ is the normal derivative of $\bar{\Phi}$ on the boundary of the /76

element ∂E. The first term on the right side of equation (8) happens to cancel out with the first half of the third term. By inserting the interpolation function (5) and transforming it into a function of (ξ,η), we get

$$S_{ij}\phi_j=F_i,\quad i=1,2,\cdots,12 \tag{9}$$

where

$$\begin{cases} S_{ij}=\dfrac{b}{a}A_{ij}+\dfrac{a}{b}B_{ij},\quad F_i=-\dfrac{b}{a}\bar{M}^2C_{ij}-aX_i, \\ A_{ij}=\displaystyle\int_{-1}^{1}\int_{-1}^{1}N_{i,\xi}N_{j,\xi}d\xi d\eta,\quad B_{ij}=\int_{-1}^{1}\int_{-1}^{1}N_{i,\eta}N_{j,\eta}d\xi d\eta, \\ C_{ij}=\displaystyle\int_{-1}^{1}\int_{-1}^{1}N_iN_{j,\xi}d\xi d\eta,\quad X_i=\int_{\partial E}N_ig'd\xi,\quad \bar{M}=\dfrac{1}{4}(M_1+M_2+M_3+M_4), \end{cases} \tag{10}$$

The local finite element equation (9) is combined into an overall equation

$$S_{kl}\phi_l^{(n)}=F_k^{(n-1)}, \tag{11}$$

where k, l=1,2,...,255. Then, we used an iterative method to solve equation (11) to obtain the nodal parameters (including derivatives). Thus, we can find the velocity $u=\phi_x$, $v=\phi_y$ and pressure coefficient $C_p=-2\phi_x$ at the node.

The matrices A_{ij}, B_{ij} and C_{ij} in the element analysis were

numerically integrated on a computer in reference [1]. It will bring about two problems: increased computer time and new error due to approximation. As a matter of fact, all the elements in these matrices can be precisely integrated. The only problem is there are too many elements and each element involves a double integral. It is just too tedious. However, an analysis shows the following patterns: 1) many elements in G_{ij} are zero; 2) all elements of B_{ij} have a certain relation with respect to the elements of A_{ij} and 3) an iterative formula can be found for A_{ij}. Thus, the integration can be greatly simplified.

From equation (6) we know that the interpolation function and its derivative are combinations of products of $(\eta-1)$, $(\eta+1)$, $(\xi-1)$ and $(\xi+1)$ of various orders. All elements of A_{ij} are double integrals of these combinations in the cubic region. After considering the separable variables of these integrals, it is only necessary to calculate the following integral:

$$I_{ab}=\int_{-1}^{1}\int_{-1}^{1}(\xi-1)^a(\eta+1)^b\,d\xi\,d\eta=(-1)^a\cdot 2^{a+b+1}\cdot\frac{a!\,b!}{(a+b+1)!}, \qquad (12)$$

By using equation (12), we can calculate all the elements of A_{ij}. For example

$$A_{11}=\int_{-1}^{1}\int_{-1}^{1}N_1 N_1\,d\xi\,d\eta=\frac{1}{32}I_{22}=\frac{1}{36}.$$

In addition, based on the symmetry of $N_i(\xi,\eta)$ with respect to ξ, η, we found the following relations exist between the elements of

B_{ij} and those of A_{ij}.

A	1	2	3		4	5	6		7	8	9	10	11	12
B	1	3	2		10	9	11		7	8	9	4	5	6

(B)

For example, $B_{2,11}=A_{3,6}$. Thus, when A_{ij} are calculated, B_{ij} are also determined. The computation of C_{ij} is similar to that of A_{ij}. It is only simpler. After all the elements of these matrices are determined, they can be stored in the computer for future use to avoid numerical integration.

II. Example and Discussion

In order to check the accuracy and efficiency of the technique, we used this method to calculate two subcritical conditions of a symmetric airfoil whose relative thickness is 6% at M_∞=0.806 and 0.861. The pressure distributions thus obtained /77 are compared to the experimental data as shown in Figure 3. The figure also shows the result obtained in reference [1]. We can see that although the meshes are divided more coarsely than in reference [1] (it was divided into 120 elements with 150 nodes in reference [1]), the accuracy of the computation is similar. They essentially agree with the experimental data.

In this paper, the computation is done on a Model M-140F minicomputer. Each state takes 3 minutes CPU time. In reference

[1], a mainframe Univac computer was used. Each state took 40 seconds. Considering the difference in the speed of these two computers, the number of operations of this method is only 45% of that used in reference [1]. Thus, we proved that the efficiency is improved with this computation under the premise that the accuracy is insured.

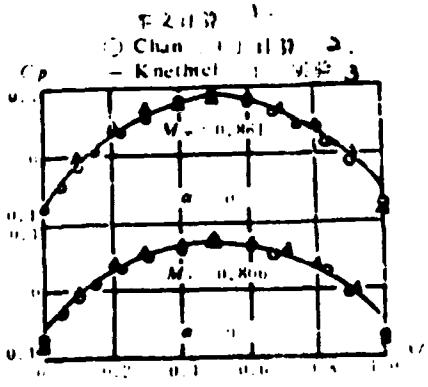

Figure 3

1. this work
2. computation by Chan in reference [1]
3. experimental data by Knechtel in reference [4]

References

[1] Chan, S.T.K., Brashears, M.R., Young, V.Y.C., AIAA 75-79, 1975.

[2] Luo Shijun et al, Hybrid Difference for Transonic Steady Flow, Defense Publishing Co., 1979.

[3] J.J. Connor, et al, Finite Methods for Fluid Flow, translated by Wu Wangyi, Science Publishing Co., 1981.

[4] Knechtel, E.D., NASA TM D- 15, 1959.

DISTRIBUTION LIST

DISTRIBUTION DIRECT TO RECIPIENT

ORGANIZATION	MICROFICHE
A205 DMATC	1
A210 DMAAC	1
B344 DIA/RTS-2C	9
C043 USAMIIA	1
C500 TRADOC	1
C509 BALLISTIC RES LAB	1
C510 AT LABS/AVRADCOM	1
C513 ARRADCOM	1
C535 AVRADCOM/TSARCOM	1
C539 TRASANA	1
C591 FSTC	4
C619 MIA REDSTONE	1
D008 NISC	1
E053 HQ USAF/INET	1
E404 AEDC/DOF	1
E408 AFWL	1
E410 AD/IND	1
E429 SD/IND	1
P005 DOE/ISA/DDI	1
P050 CIA/OCR/ADD/SD	2
AFIT/LDE	1
FTD	
CCN	1
ASD/PMS	1
LLNL/Code L-389	1
NASA/NST-44	1
NSA/1213/TDL	2
ASD/FTD/NQIA	1

END

7-87

DTIC